Article

Simultaneously Cycled NMR Spectroscopy

David M. Parish, and Thomas Szyperski

J. Am. Chem. Soc., **2008**, 130 (14), 4925-4933 • DOI: 10.1021/ja711454e

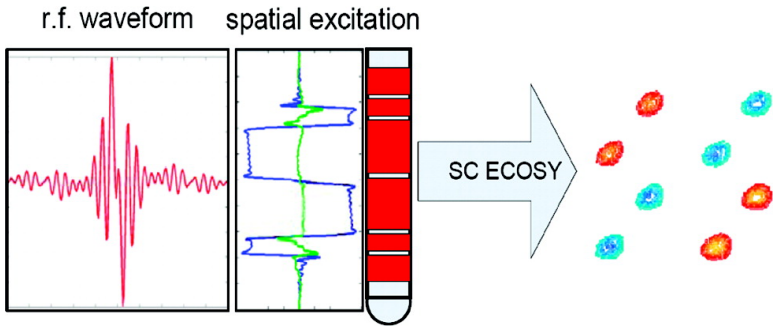

More About This Article

Additional resources and features associated with this article are available within the HTML version:

- Supporting Information
- Access to high resolution figures
- Links to articles and content related to this article
- Copyright permission to reproduce figures and/or text from this article

View the Full Text HTML

J|A|C|S
ARTICLES
Published on Web 03/14/2008

Simultaneously Cycled NMR Spectroscopy

David M. Parish and Thomas Szyperski*

Departments of Chemistry and Structural Biology, State University of New York at Buffalo, Buffalo, New York 14260

Received December 28, 2007; E-mail: szypersk@chem.buffalo.edu

Abstract: Simultaneously cycled (SC) NMR was introduced and exemplified by implementing a set of 2-D [^{1}H,^{1}H] SC exclusive COSY (E.COSY) NMR experiments, that is, rf pulse flip-angle cycled (SFC), rf pulse phase cycled (SPC), and pulsed field gradient (PFG) strength cycled (SGC) E.COSY. Spatially selective ^{1}H rf pulses were applied as composite pulses such that all steps of the respective cycles were affected simultaneously in different slices of the sample. This increased the data acquisition speed for an *n*-step cycle *n*-fold. A high intrinsic sensitivity was achieved by defining the cycles in a manner that the receiver phase remains constant for all steps of the cycle. Then, the signal resulting from applying the cycle corresponded to the sum of the signals from all steps of the cycle. Hence, the detected free induction decay did not have to be separated into the contributions arising from different slices, and read-out PFGs, which not only greatly reduce sensitivity but also negatively impact lineshapes in the direct dimension, were avoided. The current implementation of SFC E.COSY reached ~65% of the intrinsic sensitivity of the conventional phase cycled congener, making this experiment highly attractive whenever conventional data acquisition is sampling limited. Highly resolved SC E.COSY yielding accurate ^3J-coupling values was recorded for the 416 Da plant alkaloid tomatidine within 80 min, that is, 12 times faster than with conventional phase cycled E.COSY. SC NMR is applicable for a large variety of NMR experiments and thus promises to be a valuable addition to the arsenal of approaches for tackling the NMR sampling problem to avoid sampling limited data acquisition.

Introduction

Fourier transform (FT) nuclear magnetic resonance (NMR) spectroscopy[1] is one of the most widely used analytical tools in science and engineering.[2] FT NMR experiments rely on acquiring free induction decays (FIDs) that, after FT, yield the desired frequency domain spectra. Quite generally, more than a single FID has to be recorded for a given NMR experiment to suppress spectral artifacts and/or to implement multidimensional data acquisition based on sampling of indirect evolution time periods and coherence pathway selection. Particularly when considering the unprecedented sensitivity of spectrometers equipped with cryogenic probes, one nowadays routinely faces the situation that the NMR experiment time is dictated by the number of FIDs required to record a distinct type of spectrum (with sufficient resolution in indirect dimensions) and not by sensitivity limitations that require signal averaging beyond the need for radio frequency (rf) phase cycling and indirect time domain sampling.[3] To best capitalize on costly NMR hardware, one evidently prefers sensitivity limited data acquisition,[3] in which the number of FIDs (i.e., the measurement time) is chosen such that the resulting signal-to-noise (S/N) ratios are adjusted to a level ensuring reliable data interpretation while avoiding unnecessarily high S/N ratios.

NMR approaches were thus developed to accelerate NMR data acquisition.[4] Many innovations emerged in the field of biological NMR spectroscopy,[5] where stable isotope (^{13}C/^{15}N) labeled biological macromolecules are studied. The isotope labeling enables one to efficiently record three-dimensional (3-D) or four-dimensional (4-D) ^{13}C-/^{15}N-resolved spectra. In turn, the high spectral dimensionality implies a high sampling demand and long minimal measurement times, which creates an urgent demand for rapid data acquisition techniques. Widely used biological NMR techniques include (i) reduced dimensionality (RD) NMR,[3,6−8] (ii) its generalization, G-matrix FT (GFT) projection NMR[9−18] and the techniques PR NMR,[19] APSY,[20]

(1) Ernst, R. R.; Bodenhausen, G.; Wokaun, A. *Principles of Nuclear Magnetic Resonance in One and Two Dimensions*; Oxford University Press: Oxford, 1987.
(2) Jacobsen, N. E. *NMR Spectroscopy Explained*; Wiley: New York, 2007.
(3) Szyperski, T.; Yeh, D. C.; Sukumaran, D. K.; Moseley, H. N. B.; Montelione, G. T. *Proc. Natl. Acad. Sci. U.S.A.* **2002**, *99*, 8009−8014.
(4) Atreya, H. S.; Szyperski, T. *Methods Enzymol.* **2005**, *394*, 78−108.
(5) Cavanagh, J.; Fairbrother, W. J.; Palmer, A. G.; Rance, M.; Skelton, N. J. *Protein NMR Spectroscopy*; Academic Press: San Diego, 2007.
(6) Szyperski, T.; Wider, G.; Bushweller, J. H.; Wüthrich, K. *J. Am. Chem. Soc.* **1993**, *115*, 9307−9308.
(7) Brutscher, B.; Simorre, J. P.; Caffrey, M. S.; Marion, D. *J. Magn. Reson., Ser. B* **1994**, *105*, 77−82.
(8) Szyperski, T.; Banecki, B.; Braun, D.; Glaser, R. W. *J. Biomol. NMR* **1998**, *11*, 387−405.
(9) Kim, S.; Szyperski, T. *J. Am. Chem. Soc.* **2003**, *125*, 1385−1393.
(10) Atreya, H. S.; Szyperski, T. *Proc. Natl. Acad. Sci. U.S.A.* **2004**, *101*, 9642−9647.
(11) Kim, S.; Szyperski, T. *J. Biomol. NMR* **2004**, *28*, 117−130.
(12) Xia, Y. L.; Zhu, G.; S., V.; Gao, X. L. *J. Biomol. NMR* **2004**, *29*, 467−474.
(13) Atreya, H. S.; Eletsky, A.; Szyperski, T. *J. Am. Chem. Soc.* **2005**, *127*, 4554−4555.
(14) Eletsky, A.; Atreya, H. S.; Liu, G. H.; Szyperski, T. *J. Am. Chem. Soc.* **2005**, *127*, 14578−14579.
(15) Yang, S.; Atreya, H. S.; Liu, G. H.; Szyperski, T. *J. Am. Chem. Soc.* **2005**, *127*, 9085−9099.
(16) Szyperski, T.; Atreya, H. S. *Magn. Reson. Chem.* **2006**, *44*, 51−60.

and Hi-Fi NMR,[21] which are based on GFT NMR data collection, and (iii) covariance NMR spectroscopy.[22−25] Longitudinal relaxation optimization[26,27] can further accelerate data acquisition for experiments based on initial excitation and detection of polypeptide backbone amide protons[10,28,29] or aromatic proton magnetization.[14] Valuable other approaches were developed and thus far primarily applied for smaller molecules (e.g., Hadamard NMR spectroscopy[30,31] and ultrafast NMR).[32−35]

Ultrafast NMR is the only technique that allows one to record multidimensional spectra with a single scan. It is based on (i) spatiotemporal encoding of indirect chemical shift evolution followed by (ii) repetitive decoding and re-encoding during evolution of chemical shifts in the direct dimension. Step i requires the application of a train of spatially selective excitation pulses, each consisting of a shaped rf pulse in conjunction with a pulsed field gradient (PFG). This ensures that only a fraction of the sample, for example, a slice, is excited. Step ii is based on the employment of a train of PFGs with alternating signs (read-out PFGs) during signal detection, which poses high demands on the spectrometer hardware. Even if the significant loss of sensitivity associated with the application of read-out PFGs can be reduced using a single read-out PFG of constant strength,[34] the requirement to incorporate these PFGs represents a major limitation of ultrafast NMR.

In another vein, Loening et al.[36] and Bhattacharyya and Kumar[37] employed spatially selective excitation to speed up nuclear spin relaxation measurements. In these experiments, the separation of signals arising from spatially different parts of the sample was accomplished either by time-staggered acquisition or by the use of read-out PFGs. Spatially selective excitation also has been applied to high-resolution NMR for the suppression of zero-quantum coherence.[38,39]

For a large number of widely used, often 2-D [^{1}H,^{1}H] NMR experiments, it is the cycling of rf pulse phases or rf pulse flip angles for coherence selection and/or artifact suppression[1] that dictates, besides the sampling of indirect evolution periods, minimal measurement times: an *n*-step cycle implies that (at least) *n* FIDs have to be acquired and added. Hence, it appears attractive to employ spatially selective excitation to implement the simultaneous cycling of rf pulse phases or flip-angles. Most importantly, many cycling schemes can be effectively devised so that the receiver phase is constant for all steps of the cycle. Then, no read-out PFGs are required, and the joint detection of the signals from all slices directly yields the desired sum of FIDs. Here, we introduce this concept, which we name simultaneously cycled (SC) NMR, as a generally applicable NMR approach, using 2-D [^{1}H,^{1}H] exclusive correlation spectroscopy (E.COSY)[40,41] as a paradigm. First, E.COSY optimized for three-spin systems allows one to accurately measure vicinal ^{1}H−^{1}H scalar (*J*) couplings and thus plays an important role in organic and natural product chemistry. Second, E.COSY can be implemented by (i) cycling of rf pulse flip-angles,[40] (ii) cycling of rf pulse phases,[40] or (iii) co-addition of PFG coherence selected double-quantum filtered (DQF) and triple-quantum filtered (TQF) COSY spectra.[42] Since step iii requires that the strength of a PFG is varied when accomplishing DQ filtration versus TQ filtration, we refer to this approach as the PFG strength cycling. Hence, E.COSY allows one to implement and compare three types of cycling schemes, that is, rf pulse flip-angle, rf pulse phase, and PFG strength cycling. The SC E.COSY congeners named, respectively, simultaneously flip-angle cycled (SFC), simultaneously phase cycled (SPC), and simultaneously gradient strength cycled (SGC) E.COSY, were implemented and compared. This paves the way to design a large variety of SC NMR experiments with a broad potential impact in natural science and engineering.

Materials and Methods

Conventionally Cycled 2-D [^{1}H,^{1}H]-E.COSY. The rf pulse sequence of 2-D [^{1}H,^{1}H]-COSY[1] consists of two $\pi/2$ flip-angle pulses separated by the indirect evolution period t_1. To avoid dispersive diagonal peaks that may occlude nearby cross-peaks, this pulse sequence is routinely expanded by a third $\pi/2$ rf pulse right before the start of signal detection. This enables the implementation of DQF or TQF COSY.[1] E.COSY aims at simplifying the COSY cross-peak fine structure by selecting only cross-peak components representing connected transitions.[1] In turn, this allows one to accurately measure *J*-couplings.[40−43] Conventional E.COSY can be implemented in three different ways, and the corresponding rf pulse sequences are shown in Figure 1. To properly distinguish rf pulse flip-angles and phases, their values are given, respectively, in radians and degrees.

The flip-angle cycled E.COSY (Figure 1a) uses the two rf pulse sequence of COSY to acquire multiple transients with a variable flip-angle, β, for the second rf pulse. For E.COSY optimized for three-spin systems, the β angle cycle and associated receiver phases are shown in Table 1 (flip-angles are given in radians). The weighting factor for each value of β is generally applied by repeating the experiment for that number of transients to ensure that each step of the cycle is weighted with corresponding S/N. Thus, such flip-angle cycled E.COSY requires 12 transients for each increment of the indirect evolution time t_1. The phase cycled E.COSY (Figure 1b) uses the three $\pi/2$ flip-angle

(17) Atreya, H. S.; Garcia, E.; Shen, Y.; Szyperski, T. *J. Am. Chem. Soc.* **2007**, *129*, 680−692.
(18) Xia, Y. L.; Veeraraghavan, S.; Zhu, Q.; Gao, X. *J. Magn. Reson.* **2008**, *190*, 142−148.
(19) Kupce, E.; Freeman, R. *J. Am. Chem. Soc.* **2004**, *126*, 6429−6440.
(20) Hiller, S.; Fiorito, F.; Wuthrich, K.; Wider, G. *Proc. Natl. Acad. Sci. U.S.A.* **2005**, *102*, 10876−10881.
(21) Eghbalnia, H. R.; Bahrami, A.; Tonelli, M.; Hallenga, K.; Markley, J. L. *J. Am. Chem. Soc.* **2005**, *127*, 12528−12536.
(22) Bruschweiler, R. *J. Chem. Phys.* **2004**, *121*, 409−414.
(23) Bruschweiler, R.; Zhang, F. *J. Chem. Phys.* **2004**, *120*, 5253−5260.
(24) Zhang, F.; Bruschweiler, R. *J. Am. Chem. Soc.* **2004**, *126*, 13180−13181.
(25) Chen, Y.; Zhang, F.; Bermel, W.; Bruschweiler, R. *J. Am. Chem. Soc.* **2006**, *128*, 15564−15565.
(26) Pervushin, K.; Vogeli, B.; Eletsky, A. *J. Am. Chem. Soc.* **2002**, *124*, 12898−12902.
(27) Deschamps, M.; Campbell, I. D. *J. Magn. Reson.* **2006**, *178*, 206−211.
(28) Schanda, P.; Van Melckebeke, H.; Brutscher, B. *J. Am. Chem. Soc.* **2006**, *128*, 9042−9043.
(29) Gal, M.; Schanda, P.; Brutscher, B.; Frydman, L. *J. Am. Chem. Soc.* **2007**, *129*, 1372−1377.
(30) Bircher, H. R.; Muller, C.; Bigler, P. *J. Magn. Reson.* **1990**, *89*, 146−152.
(31) Blechta, V.; Freeman, R. *Chem. Phys. Lett.* **1993**, *215*, 341−346.
(32) Frydman, L.; Scherf, T.; Lupulescu, A. *Proc. Natl. Acad. Sci. U.S.A.* **2002**, *99*, 15858−15862.
(33) Frydman, L.; Lupulescu, A.; Scherf, T. *J. Am. Chem. Soc.* **2003**, *125*, 9204−9217.
(34) Shrot, Y.; Frydman, L. *J. Chem. Phys.* **2006**, *125*, 204507 (12 pages).
(35) Mishkovsky, M.; Gal, M.; Frydman, L. *J. Biomol. NMR* **2007**, *39*, 291−301.
(36) Loening, N. M.; Thrippleton, M. J.; Keeler, J.; Griffin, R. G. *J. Magn. Reson.* **2003**, *164*, 321−328.
(37) Bhattacharyya, R.; Kumar, A. *Chem. Phys. Lett.* **2004**, *383*, 99−103.
(38) Thrippleton, M. J.; Keeler, J. *Angew. Chem., Intl. Ed.* **2003**, *42*, 3938−3941.
(39) Cano, K. E.; Thrippleton, M. J.; Keeler, J.; Shaka, A. J. *J. Magn. Reson.* **2004**, *167*, 291−297.
(40) Griesinger, C.; Sørensen, O. W.; Ernst, R. R. *J. Chem. Phys.* **1986**, *85*, 6837−6852.
(41) Griesinger, C.; Sorensen, O. W.; Ernst, R. R. *J. Magn. Reson.* **1987**, *75*, 474−492.
(42) Willker, W.; Lieibfritz, D.; Kerssebaum, R.; Lohman, J. *J. Magn. Reson., Ser. A* **1992**, *102*, 348−350.
(43) Schroder, F. C.; Tolasch, T. *Tetrahedron* **1998**, *54*, 12243−12248.

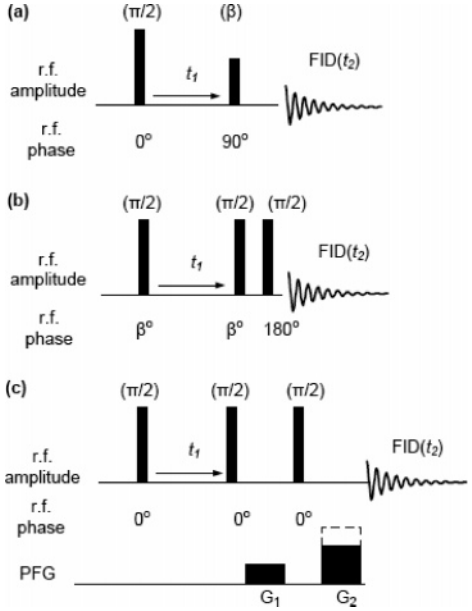

Figure 1. rf pulse schemes for conventional E.COSY.[40−42] Rectangular high-powered ^{1}H pulses are indicated by vertical bars. The flip-angles (rad) and phases (deg) are indicated, respectively, above and below the bars and are provided in Table 1. The indirect and direct chemical shift evolution periods are denoted as t_1 and t_2, respectively. In panel a, a 12-step cycle was employed for the flip angle of the second rf pulse along with the receiver phase according to values provided in Table 1. In panel b, a 12-step cycle was employed for the rf pulse phases along with the receiver phases according to the values of Table 1. In panel c, a three-step cycle was employed for the strength of PFG2, which was set to 3 times the strength of PFG1 for two steps and to twice the strength of PFG1 for one step. For the current study, the duration and amplitude of PFG1 were 300 μs and 20 G/cm, respectively.

Table 1. Flip-Angle or Phase Cycle for Conventional E.COSY Optimized for a Three-Spin System

flip-angle β (rad)	0	$\pi/3$	$2\pi/3$	$4\pi/3$	$5\pi/3$
pulse phase β (deg)	0	60	120	240	300
receiver phase (deg)	0	180	0	0	180
weight factor (number of transients)	4	3	1	1	3

pulse sequence of DQF/TQF COSY, and multiple transients were acquired with varying rf pulse phases. The phase angles of the first two $\pi/2$ rf pulses, which are likewise denoted here as β, take on the same values and number of transients as the flip-angles β in the flip-angle cycled E.COSY. In fact, flip-angle and phase angle cycled E.COSY are equivalent for ideal rf pulses.[40] As in flip-angle cycled E.COSY, the weighting factor determines the number of FIDs recorded for a given value of β, thus likewise resulting in a minimum of 12 transients to implement the phase or flip-angle cycle for an E.COSY optimized for three-spin systems (a minimum of 32 transients is required for E.COSY optimized for four-spin systems). Evidently, a further extended phase cycle is required if artifact suppression is desired in addition to the coherence selection.

E.COSY optimized for three-spin systems represents a sum of DQF COSY and 2 times TQF COSY [if DQF and TQF are accomplished by rf pulse phase cycling, the resulting phase cycle would then be longer than what is required for direct E.COSY acquisition (Table 1)]. Since single-transient DQF and TQF COSY can be implemented by using PFGs for coherence pathway selection,[44] PFG coherence selected E.COSY represents the third way to implement E.COSY[42] (Figure 1c). This is accomplished by recording one transient with DQ filtration and two transients with TQ filtration, for which the rephasing PFG2 (Figure 1c) is adjusted, respectively, to 2 or 3 times the strength of dephasing

(44) Hurd, R. E. *J. Magn. Reson., Ser. A* **1990**, *87*, 422−428.

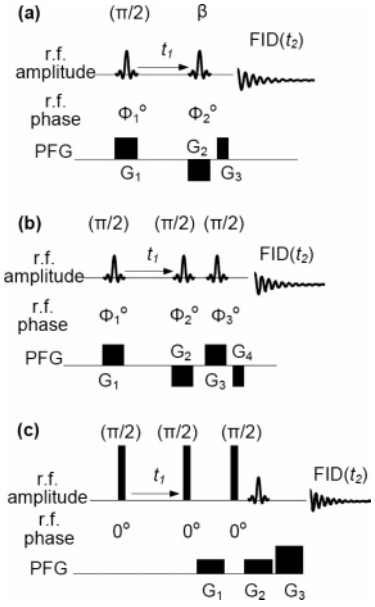

Figure 2. rf pulse schemes for SC E.COSY. Rectangular high-powered ^{1}H pulses are indicated by vertical bars. Selective ^{1}H pulses are represented by a sinc function indicating their shape and were applied concomitantly with PFGs indicated below the rf pulses and are thus spatially selective (for details, see Figure 3). The flip-angles (rad) and phases (deg) are indicated, respectively, above and below the rf pulses. The values of β and Φ are provided in Tables 2 and 3. (a) SFC E.COSY: PFG1, 270 μs, 47 G/cm; PFG2, 270 μs, −47 G/cm; and PFG3, 135 μs, 50 G/cm. (b) SPC E.COSY: PFG1, 270 μs, 47 G/cm; PFG2, 270 μs, −47 G/cm; PFG3, 270 μs, 47 G/cm; and PFG4, 150 μs, 45 G/cm. (c) SGC E.COSY: PFG1, 100 μs, 22.55 G/cm; PFG2, 120 μs, 18.8 G/cm; and PFG3, 125 μs, 35 G/cm.

Table 2. Pulse Phases and Flip-Angles for SFC E.COSY Optimized for a Three-Spin System

slice	1	2	3	4	5	6
pulse 1 phase Φ_1 (deg)	0	0	180	180	0	0
pulse 2 flip-angle β (rad)	0	$2\pi/3$	$\pi/3$	$\pi/3$	$2\pi/3$	0
pulse 2 phase Φ_2 (deg)	90	90	−90	90	−90	90
receiver phase[a] (deg)	0	0	0	0	0	0
slice thickness	2	1	3	3	1	2

[a] Constant receiver phase is required to avoid read-out gradients.

PFG1. Since this corresponds to cycling the strength of PFG2, we refer to this E.COSY implementation as a gradient strength cycled E.COSY (Figure 1c), which requires the acquisition of three transients. Importantly, however, PFG-based coherence selection reduces the intrinsic sensitivity of DQF, TQF, and thus E.COSY by a factor of 2.[42] This makes the flip-angle cycled or rf pulse phase cycled implementation the preferred choice for many applications.

SC 2-D [^{1}H,^{1}H]-E.COSY. Simultaneously flip-angle, phase angle, and gradient strength cycled E.COSY (Figure 2) were implemented using the basic concepts to implement SC NMR devoid of read-out PFGs, that is (i) selective excitation of fractions of the NMR sample with each fraction being used to execute an individual step of the cycle and (ii) design of a cycle having a constant receiver phase (e.g., zero) for all steps. This ensures that the signal detected simultaneously from all slices represents the sum of FIDs required for E.COSY. For the present implementations, discrete slices within the NMR-active sample volume oriented orthogonally to the *z*-axis defined by the magnetic field $\boldsymbol{B}_0$ were spatially selectively excited, and the relative thickness of the slices was chosen to reflect the weighting factors (Table 2). Notably, the finite duration of PFG pulses requires that first-order phase corrections are applied during data processing. Compensating spin−echo modules could be incorporated to remove these corrections. However, this would lead to some loss of intrinsic sensitivity and was

thus not pursued when designing the SC E.COSY schemes (Figure 2) described in detail in the following sections.

SFC E.COSY. For SFC E.COSY (Figure 2a), both rf pulses need to be spatially selective to ensure that the receiver phase can be set to zero for all steps of the cycle. Each of the two rf pulses affected six different slices with different rf pulse flip-angles, β, and phases, Φ_1 and Φ_2, to execute the required flip-angle cycle with a single transient. The values for β, Φ_1, and Φ_2 were derived from the conventional cycle (Table 1) [i.e., for steps with $\beta = \pi + \alpha > \pi$, the phase of the rf pulse was changed by 180°, and the flip-angle was set to $\pi - \alpha$, while for steps with a 180° receiver phase shift, that phase shift was instead applied to both rf pulses (Table 2)]. Two composite rf pulses were then created as the sum of individual rf pulses affecting individual slices. These simultaneously excite the six slices with flip-angles, phases, and slice thicknesses as shown in Table 2. The temporal waveforms and experimentally determined spatial excitation profiles of the two selective pulses of SFC E.COSY (Figure 2a) are shown, respectively, in Figure 3a,b (waveform and excitation profile of the first rf pulse) and Figure 3c,d (waveform and excitation profile of the second rf pulse). A technical comment relates to the fact that the PFG strengths need to be accurately adjusted to ensure that desired coherences are not partially dephased. The strengths of PFG 1 and PFG 2 were adjusted to select the desired slice thicknesses given the spectral width of the spatially selective rf pulse. PFG 2 was inverted so as to rephase the dephasing of desired coherences by PFG 1, and the excess dephasing of PFG 2 was rephased by PFG 3.[45]

SPC E.COSY. For SPC E.COSY (Figure 2b), three spatially selective $\pi/2$ flip-angle rf pulses were applied, affecting six different slices with different pulse phases Φ_1, Φ_2, and Φ_3 (Table 3). The values for Φ were derived from the conventional cycle (Table 1) by increasing the rf pulse phases for steps with a receiver phase of 180° by that amount. This ensures that the receiver phase can be set to zero for all slices (Table 3). Three composite rf pulses were then created as the sum of individual rf pulses affecting individual slices. The temporal waveforms and experimentally determined spatial excitation profiles of the first and third selective rf pulses of SPC E.COSY (Figure 2b) are shown, respectively, in Figure 3e−h. The second rf pulse is the same as the first one, except for a reversal of the order of slices to compensate for the reversal of the gradient polarity for PFG 2. The PFG strengths in SPC E.COSY likewise need to be set accurately. The strengths of PFG 1, PFG 2, PFG 3, and PFG 4 were adjusted to select the desired slice thicknesses given the spectral width of the spatially selective rf pulse and to ensure that overall dephasing and rephasing of the PFGs are equal.

SGC E.COSY. For SGC E.COSY, the conventional rf pulse sequence (Figure 1c) was modified by introducing a spatially selective π pulse right before signal detection (Figure 2c) and relies on the fact that dephasing of coherences by PFGs can be effectively rephased by applying a π −pulse.[5] In general, a spatially selective π pulse in the middle of a train of one or more PFG pulses will produce a net gradient pulse in the region that is affected by the π pulse equal to the total PFG strength prior to the π pulse minus the total PFG strength following the π pulse. In contrast, coherences in slices not affected by the selective π pulse receive a net gradient pulse equal to the sum of the strengths of all of the pulses in the pulse train. As a result, different slices experience different PFG strengths so that PFG strength cycling can be implemented. For E.COSY optimized for three-spin systems, the sum of a DQF and 2 times a TQF COSY needs to be acquired. Hence, a spatially selective π rf pulse in the middle of PFG 2 followed by PFG 3 having twice the strength of PFG 1 is introduced. The slice thickness of the spatially selective π pulse was adjusted so that one-third of the sample experienced no net gradient from PFG 2. Hence, only double quantum coherences were rephased by PFG3 in this slice, while the remaining two-thirds of the sample was not affected by the π pulse so that PFG2 and PFG3 serve to rephase triple-quantum coherences. The resulting signal yielded the desired SGC E.COSY spectrum. The temporal waveform and experimentally determined spatial excitation profile for the spatially selective π pulse used for SGC E.COSY are shown, respectively, in Figure 3i,j, respectively.

Composite rf Pulses for SC E.COSY. The selective rf pulses required for implementing SC NMR (Figure 3) are pivotal for this approach. Composite shaped rf pulses were generated using the program Matlab (The MathWorks Inc.). The temporal rf pulse shapes corresponding to each slice, with a desired slice thickness and offset from center, were individually generated and then added to create the composite rf pulse.

The temporal shape, $S_1(t)$, of the rf pulse exciting only the thinnest slice 1 (defining a relative width of 1.0) was represented by the three central lobes of a sinc function, that is, $S(t) = \sin(t)/t$ for $-3\pi < t < 3\pi$ digitized with 200 points and having a time−bandwidth product[46] of 6. Hence, the rf pulse selectively exciting slice 2 with a relative thickness 2.0 is given by $S_2(t) = \sin(t)/t$ for $-6\pi < t < 6\pi$ digitized with 200 points. To shift the center of excitation of the second pulse by a relative distance of 1.65 so as to make it adjacent to slice 1 with 110% spacing of the centers of excitation to mitigate slice-to-slice interference, $S_2(t)$ was time shifted according to $S_{2,\mathrm{offset}}(t) = S_2(t)\exp(i1.65 \times 2t)$ for $-3\pi < t < 3\pi$ with 200 points. The shapes $S_{n,\mathrm{offset}}(t)$ of rf pulses exciting additional slices were generated accordingly, and the summation of all individual shapes yielded the shape for the composite rf pulse, $S_{\mathrm{comp}}(t)$. Since the desired excitation profile for each of the individual rf pulses was Hermitian (the profile is its own conjugate transpose), the temporal shapes possessed no imaginary components. The composite rf pulses become spatially selective by applying them concurrently with a z-axis PFG, and the rf pulse bandwidth divided by the amplitude of the PFG yielded the thickness Δz of the excited slice, where the pulse bandwidth is given by the time−bandwidth product divided by the pulse duration.[47]

Excitation profiles (Figure 3) were experimentally determined by applying the composite rf pulse with shape $S_{\mathrm{comp}}(t)$ to a sample of ~1% H_2O dissolved in D_2O. During acquisition, a z-axis read-out PFG was applied (which encodes the z-axis position as frequency) so that a FT of the acquired signal yielded the spatial excitation profile. For the selective π pulse (Figure 3i,j), a rectangular $\pi/2$ pulse was applied before the π pulse, which then selectively inverted the transverse magnetization.

NMR Data Collection, Processing, and Analysis. COSY spectra were recorded with two samples, that is (i) a 100 mM solution of the proteinogenic amino acid tyrosine dissolved in D_2O at pD = 10 and (ii) a 30 mM solution of the plant solanum-steroid-alkaloid tomatidine[48,49] [(3β,5α,25S)-spirosolan-3-ol; CAS no. 77−-59-8)] dissolved in pyridine. Data were acquired on a Varian INOVA 500 spectrometer equipped with a conventional $^1H\{^{13}C,^{15}N,^{19}F\}$ probe, processed using the program NMRPipe[50] and analyzed using the program NMRDraw.[50]

Results and Discussion

SC E.COSY experiments (Figure 2) were implemented and compared in terms of intrinsic sensitivity and performance using a 100 mM solution of the proteinogenic amino acid tyrosine in D_2O. Tyrosine contains two diasterotopic ^2J-coupled β protons

(45) During about the first half of PFG 1, the magnetization is largely longitudinal and thus not affected by the PFG.

(46) Schulte, R. F.; Henning, A.; Tsao, J.; Boesiger, P.; Pruessmann, K. P. *J. Magn. Reson.* **2007**, *186*, 167−175.
(47) During selective excitation, the chemical shifts of different nuclei within the sample will result in a different spatial offset of the selected slice for each nuclei. However, in the presence of PFGs with strengths employed for the present study (Figure 2), this offset is negligibly small even for chemical shifts of tens of parts per million.
(48) Willker, W.; Leibfritz, D. *Magn. Reson. Chem.* **1992**, *30*, 645−650.
(49) Raffauf, R. F. *Plant Alkaloids: A Guide to Their Discovery and Distribution*; Haworth Press: Binghamton, 1996.
(50) Delaglio, F.; Grzesiek, S.; Vuister, G. W.; Zhu, G.; Pfeifer, J.; Bax, A. *J. Biomol. NMR* **1995**, *6*, 277−293.

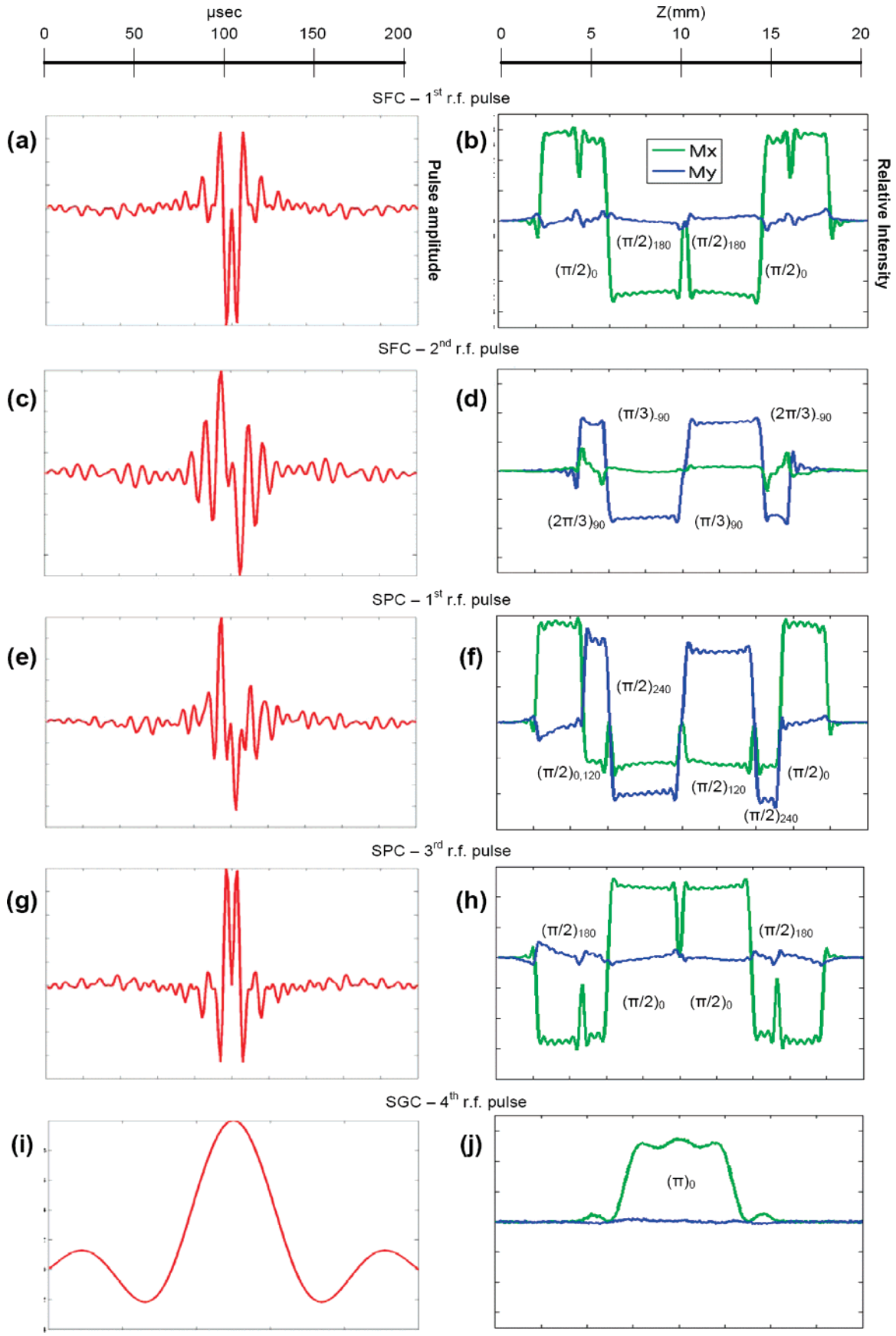

Figure 3. Temporal rf pulse shapes and their experimentally determined spatial excitation profiles (see text) along the magnetic $\boldsymbol{B}_0$ field defining the z-axis. (a and b) SFC: first rf pulse, temporal waveform, and excitation profile (green represents $\boldsymbol{M}_x$ and blue represents $\boldsymbol{M}_y$), respectively; (c and d) SFC: second rf pulse; (e and f) SPC: first rf pulse; the second rf pulse shows a profile that is reverse to the one of the first rf pulse; (g and h) SPC: third rf pulse; and (i and j) SGC: selective rephasing pulse.

Table 3. Pulse Phases for SPC E.COSY Optimized for a Three-Spin System

slice	1	2	3	4	5	6
pulse 1 phase Φ_1 (deg)	0	120	240	120	240	0
pulse 2 phase Φ_2 (deg)	0	240	120	240	120	0
pulse 3 phase Φ_3 (deg)	180	180	0	0	180	180
receiver phase[a] (deg)	0	0	0	0	0	0
slice thickness	2	1	3	3	1	2

[a] Constant receiver phase is required to avoid read-out gradients (Figure 2).

with nondegenerate chemical shifts that are themselves coupled by $^3J_{\alpha\beta}$-couplings solely to the α proton. Hence, the $^1H^{\alpha}-^1H^{\beta 2}-^1H^{\beta 3}$ spin system of tyrosine allows one to accurately compare the intrinsic sensitivity and quality of E.COSY peak pattern detection. The thus optimized implementations were applied to obtain E.COSY spectra for a 30 mM solution of the 416 Da plant alkaloid tomatidine dissolved in pyridine. Tomatidine exhibits ^1H chemical shifts dispersed over a range of ~4.2 ppm, and the resulting high-quality SC E.COSY NMR spectra demonstrate the versatility of SC NMR for routine applications in organic and natural product chemistry.

Performance of SC E.COSY: Spectra Recorded for Tyrosine. Figure 4 shows spectral regions of E.COSY spectra comprising the cross-peaks detected on $^1H^{\beta 2}$ and $^1H^{\beta 3}$ of tyrosine. As a reference, peaks were simulated with known chemical shifts and scalar couplings using the program QSIM[51] (Figure 4a). Regions taken from conventional rf pulse phase cycled (measurement time: 285 min) and PFG coherence selected E.COSY spectra (measurement time: 72 min) are shown in Figure 4b,c, respectively. Comparison with SFC (Figure 4d), SPC (Figure 4e), and SGC E.COSY (Figure 4f) spectra recorded within 24 min shows that the SC NMR data acquisition allows accurate selection of the desired E.COSY cross-peak fine structure with all three SC E.COSY schemes (Figure 2).

Furthermore, the S/N ratios were measured for these cross-peaks, and in order to compare intrinsic sensitivity, these ratios were divided by the square root of the acquisition time (Table 4). For conventional phase cycled and gradient selected E.COSY, normalized S/N ratios of 46 and 16 were obtained, respectively. As expected,[42] the incorporation of the two additional PFGs for coherence selection reduced the intrinsic sensitivity somewhat below the theoretically predicted factor of 2. For SC E.COSY, the normalized S/N ratios (Table 4) turned out to be 30 for SFC (65% of conventional phase cycled E.COSY), 17 for SPC (37% of conventional phase cycled E.COSY), and 13 for SGC E.COSY (76% of conventional PFG coherence selected E.COSY). For SFC and SPC E.COSY, the loss of intrinsic sensitivity relative to conventional E.COSY was primarily due to (i) imperfections of shaped rf pulses, (ii) imperfect rephasing of desired coherences, and (iii) the fact that the spatially selected slices are separated by gaps that do not contribute to the detected signal (Figure 3). However, since the intrinsic sensitivity of currently implemented SFC E.COSY (Figure 2a) reaches 65% of what is registered for conventionally phase cycled E.COSY, it is evident that this SC NMR experiment is valuable for routine applications. The rather low intrinsic sensitivity of SPC E.COSY is due to the fact that three spatially selective rf pulses are required (Figure 2b). It is likely that the sensitivity for each of the SC methods can be improved by refining the composite rf pulses using convex optimization[52,53] or direct waveform synthesis.[54]

The observed intrinsic sensitivities (Table 4) are in agreement with Bloch simulations,[55] which predict that each spatially selective rf pulse acting on either longitudinal magnetization or on transverse magnetization reduces the intrinsic sensitivity by about 20%. Hence, a prime goal when designing SC NMR experiments must be to reduce the number of selective rf pulses to a minimum. The relatively high sensitivity of SGC E.COSY (76% relative to the conventional PFG coherence selected E.COSY) is due to the fact that only about a third of the sample receives any selective pulse at all. While this portion of the sample does incur some loss (about 20%) due to the imperfect nature of the selective π rf pulse, the remaining 2/3 of the sample contributes the same amount of signal as in the conventional study. Note, however, that SGC E.COSY is per se a factor of 2 less sensitive than the SFC and SPC congeners.

Overall, SFC E.COSY is the most sensitive of the SC E.COSY experiments presented here. A practical advantage of least sensitive SGC E.COSY is that it is most robust with respect to inaccurate PFG calibration because PFG DQ and TQ filtration per se efficiently suppresses undesired dispersive peak components.

Application of SFA E.COSY: Spectrum Acquired for the Alkaloid Tomatidine. A highly resolved SFC E.COSY spectrum ($t_{1,max} = 410$ ms and $t_{2,max} = 614$ ms) was recorded in 80 min for tomatidine (Figure 5a). For comparison, a conventional phase cycled E.COSY spectrum was recorded, which required 960 min of measurement time (see Supporting Information), that is, 12 times longer. Representative cross-peaks exhibit S/N ratios of ~200 in this spectrum, demonstrating that conventional data acquisition is pursued in the sampling limited acquisition regime. In SFA E.COSY, cross-peak detection is complete, and the corresponding S/N ratios in the SFA E.COSY experiment are still ~50. Because of the high spectral resolution, this enables one to accurately measure ^3J-couplings.

In contrast to SFA E.COSY, the measurement of J-couplings in conventional phase cycled DQF COSY (Figure 5b; 320 min measurement time) was impeded by intricate cross-peak fine structures: the cross-peak arising from the spin system that is detected on $^1H^{15\alpha}$ (2.03 ppm; Figure 5a, inset i) enables accurate measurement of $^3J(14\text{-}15\beta) = 14.0$ Hz in E.COSY only (a cross-section taken along ω_2 shows that the peak components corresponding to undesired transitions were almost completely eliminated). Similarly, the cross-peak arising from the spin system detected on $^1H^{4\beta}$ (1.55 ppm; Figure 5, inset ii) yields accurate measurements of $^3J(4\alpha\text{-}3) = 5.9$ Hz.

Design of Suite of SC NMR Experiments. The principles of SC NMR set forth in this article allow one to design a suite of SC NMR experiments for a large range of different

(51) Helgstrand, M.; Allard, P. *J. Biomol. NMR* **2004**, *30*, 71−80.

(52) Conolly, S.; Nishimura, D.; Macovski, A. *IEEE Trans Med Imaging* **1986**, *MI-5*, 106−115.

(53) Kessler, H.; Mronga, S.; Gemmecker, G. *Magn. Reson. Chem.* **1991**, *29*, 527−557.

(54) Pauly, J.; Le Roux, P.; Nishimura, D.; Macovski, A. *IEEE Trans Med Imaging* **1991**, *10*, 53−65.

(55) A single-spin Bloch simulation was implemented using Matlab. The simulation assumed ideal rf pulses and PFG waveforms. Spatially selective rf pulses were applied, and the desired component of the final magnetization was integrated over the spatially selective slice and compared to a perfect transfer of magnetization.

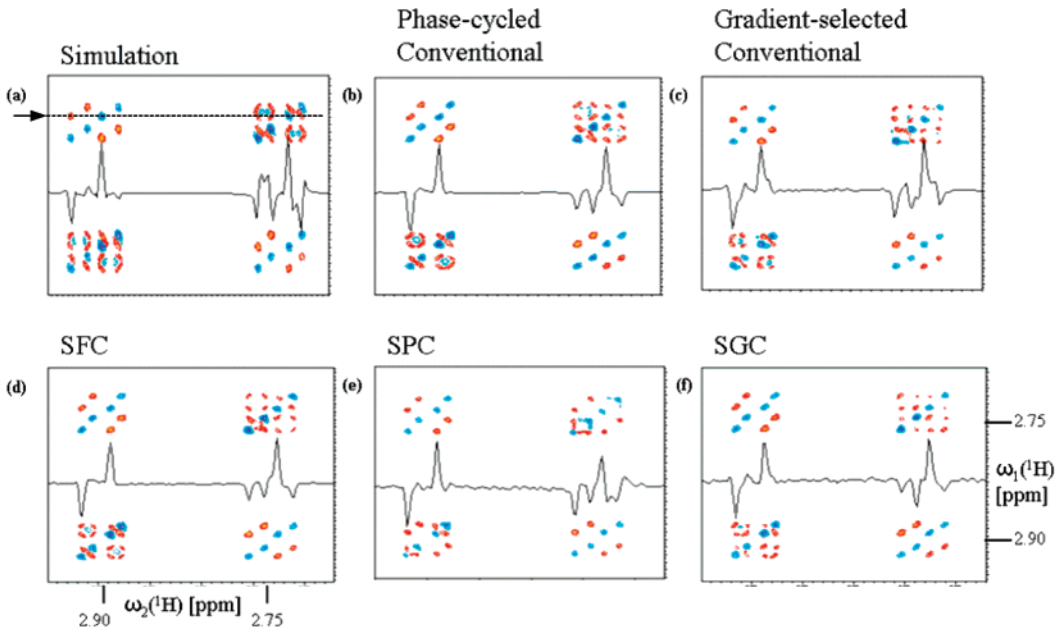

Figure 4. Spectral regions comprising peaks detected on $^1H^{\beta 2}$ and $^1H^{\beta 3}$ of tyrosine taken from (a) a simulation and (b−f) E.COSY spectra (as indicated above the panels) recorded with 256 complex points and 500 Hz spectral width in both dimensions (t_{max} = 512 ms) and a relaxation delay, τ_{rel}, between scans of 2 s yielding a total relaxation time of 2.51 s. The time−domain data were multiplied with cosine functions and zero-filled 2 times before FT, which resulted in a digital resolution of 0.98 Hz/point. (a) QSIM[51] simulation, (b) phase cycled conventional E.COSY (Figure 1b), (c) PFG coherence selected conventional E.COSY (Figure 1c), (d) SFC E.COSY (Figure 2a), (e) SPC E.COSY (Figure 2b), and (f) SGC E.COSY (Figure 2c).

Table 4. Signal-to-Noise Ratio for Conventional and Simultaneous Cycled E.COSY

experiment	no. of transients	S/N	S/N/$\sqrt{t}$[a]
	Conventional E.COSY		
phase cycled	12	160	46
PFG selected	3	28	16
	SC E.COSY		
flip-angle cycled	1	30	30
phase cycled	1	17	17
gradient selected	1	13	13

[a] t defines the total measurement time.

applications, except when independent acquisition of the signals of the cycle steps is required as in, for example, pure absorption mode quadrature detection.[1,5]

First, considering the corresponding flip-angle or phase cycles,[40,41] it is straightforward to extend the SC E.COSY cycling (optimized here for three-spin systems) to larger spin systems.

Second, all 2-D [^{1}H,^{1}H] NMR experiments consisting of two or three rf pulses are amenable to SC NMR in a straightforward manner, as exemplified here for E.COSY. Those include all variations of 2-D multiple-quantum and multiple-quantum filtered NMR experiments[1] as well as 2-D [^{1}H,^{1}H] NOESY.[1,5] The latter experiment represents a particularly attractive choice in cases where long proton T_1 relaxation times require long relaxation delays between scans to prevent that ^{1}H−^{1}H NOE intensities are affected by largely varying individual ^{1}H steady-state magnetizations. For example, 2-D [^{1}H,^{1}H] NOESY for the structure determination of RNA is usually acquired with 5−10 s delay between scans.[56−58] If a PFG is applied during the mixing time of 2-D [^{1}H,^{1}H] NOESY, the phases ϕ_1, ϕ_2, and ϕ_3 of the three ^{1}H rf pulses and the receiver phase ϕ_{Rec} are conventionally cycled for axial peak suppression as[59] ϕ_1 = 0, 180°; ϕ_2 = 0, 0°; ϕ_3 = 0, 0°; and ϕ_{Rec}= 0, 180°. The corresponding SC NMR phase cycle for 2-fold increased data acquisition speed then needs to be ϕ_1 = 0, 0°; ϕ_2 = 0, 180°; ϕ_3 = 0, 180°; and ϕ_{Rec}= 0, 0° to keep the receiver phase constant.

Third, heteronuclear SC NMR experiments can be devised considering that (i) the number of selective ^{1}H rf pulses need to be kept minimal, (ii) an even number of π rf pulses can be applied nonselectively since ^{1}H magnetization is then flipped back along z, and (iii) rf pulses on other spins that are not cycled can be applied nonselectively as long as the polarization transfer starts and ends on protons. An obvious example for such a heteronuclear SC NMR experiment would be a heteronuclear multiple-quantum correlation (HMQC) experiment,[5] which relies on only two ^{1}H and two ^{15}N rf pulses. Conventionally,[5] the minimal phase cycle involves phase ϕ_1 of the first ^{15}N rf pulse and the receiver phase ϕ_{Rec}, that is (ϕ_1 = 0, 180° and ϕ_{Rec}= 0, 180°). The corresponding SC NMR phase cycle for the 2-fold increased data acquisition speed needs to cycle ϕ_1 along with the phase ϕ_2 of the first ^{1}H rf pulse instead (i.e., ϕ_1 = 0, 180°; ϕ_2 = 0, 180°; and ϕ_{Rec}= 0, 0°) to keep the receiver phase constant.

Conclusion

SC NMR enables one to simultaneously execute cycles of rf pulse flip-angles, rf pulse phases, or PFG strengths. The minimal measurement time of an NMR experiment performed with an n-step cycle is thus reduced n-fold, indicating that SC NMR represents a valuable addition to the arsenal of approaches for tackling the NMR sampling problem.[4] Since read-out PFGs and their associated increased sampling rate are avoided, a largely

(56) Varani, G.; F., A.-e.; Allain, F. H. T. *Prog. Nucl. Magn. Reson. Spectrosc.* **1996**, *29*, 51−127.
(57) Szyperski, T.; Gotte, M.; Billeter, M.; Perola, E.; Cellai, L.; Heumann, H.; Wüthrich, K. *J. Biomol. NMR* **1999**, *13*, 343−355.
(58) Hantz, E.; Larue, V.; Ladam, P.; Le Moyec, L.; Gouyette, C.; Dinh, T. H. *Int. J. Biol. Macromol.* **2001**, *28*, 273−284.
(59) Braun, S.; Kalinowski, H.; Berger, S. *150 and More Basic NMR Experiments*; Wiley-VCH: Weinheim, Germany, 1998.

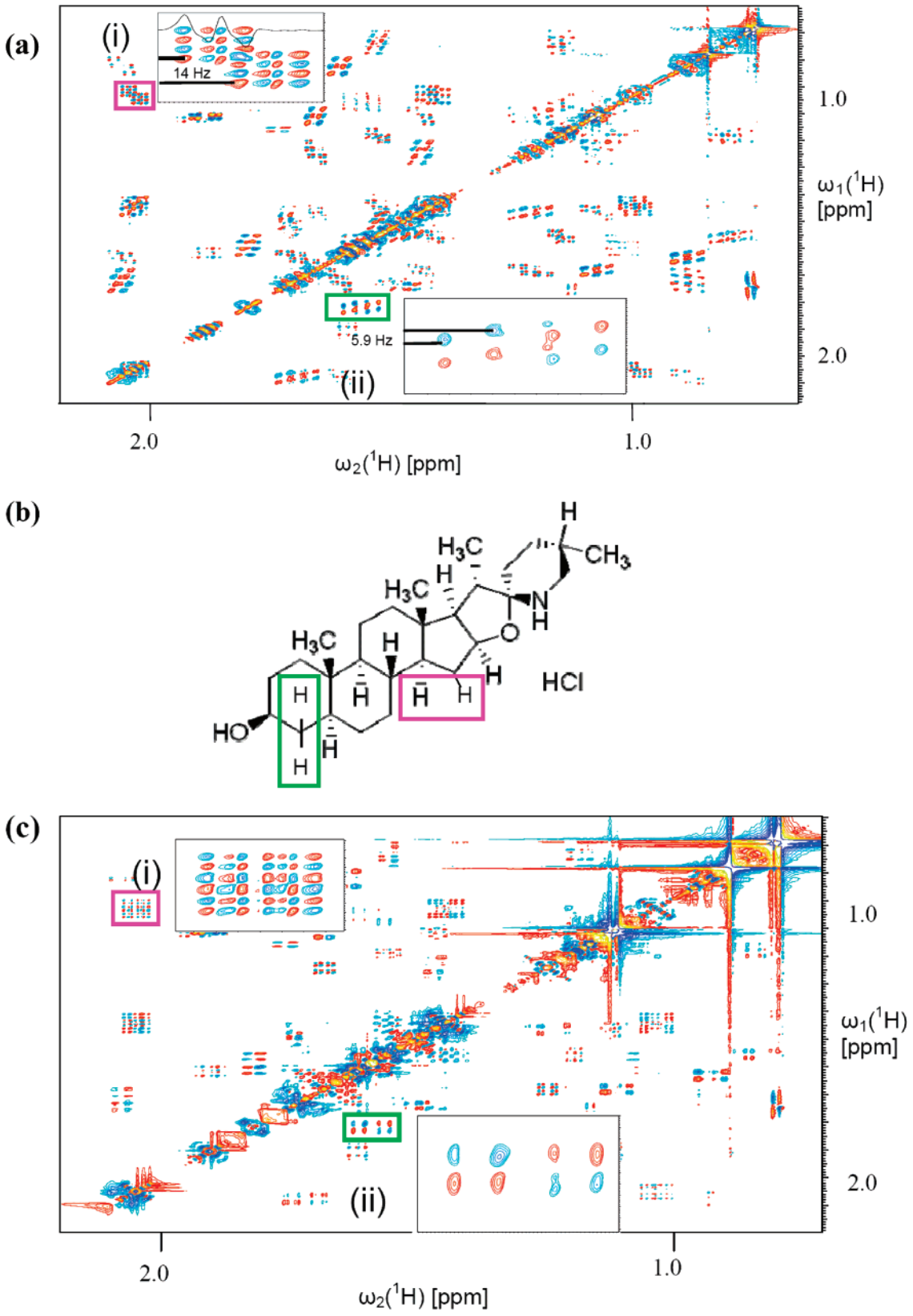

Figure 5. (a) Spectral region taken from SFC E.COSY recorded for plant alkaloid tomatidine[48] with 1024 complex points along t_1, 1536 complex points along t_2, and 2500 Hz spectral width in both dimensions yielding $t_{1,max} = 410$ ms and $t_{2,max} = 614$ ms and a delay, τ_{rel}, between scans of 1.5 s, yielding a total T_1 relaxation delay of 2.1 s. The time−domain data were multiplied with a cosine function and zero-filled 4 times in both dimensions, yielding after FT a digital resolution of, respectively, 0.6 and 0.4 Hz/point for ω_1 and ω_2. Expanded cross-peaks used to measure J-couplings (see text) are shown in the two insets. (b) A conventional DQF COSY spectrum[1] recorded with the same spectral resolution is shown for comparison.

increased intrinsic sensitivity is achieved when compared with ultrafast NMR.[33] For the same reason, SC NMR offers the same lineshapes and thus the same high resolution in the detected dimension as conventional experiments, whereas ultrafast NMR

may suffer from compromised spectral widths, resolution, and linewidths due to finite PFG strength and PFG drooping.[33] Furthermore, we have shown here that the careful design of selective rf pulses results in an intrinsic sensitivity for SC NMR experiments with two or three selective rf pulses, which is quite comparable to the sensitivity of their conventional congeners. Finally, the acquisition speed of SC NMR can be further increased by sparse data sampling[60−62] or covariance NMR processing.[22] Taken together, SC NMR promises to impact NMR data acquisition in various areas of research, including chemistry, engineering, and biology.

Acknowledgment. This work was supported by the National Science Foundation (MCB 0416899).

Supporting Information Available: (i) Plot of entire SFC 2-D [^{1}H,^{1}H]-E.COSY; (ii) conventional phase cycled 2-D [^{1}H,^{1}H]-E.COSY; and (iii) [^{1}H,^{1}H]-DQF COSY spectra recorded for tomatidine. This material is available free of charge via the Internet at http://pubs.acs.org.

JA711454E

(60) Schmieder, P.; Stern, A. S.; Wagner, G.; Hoch, J. C. *J. Biomol. NMR* **1993**, *3*, 569−576.
(61) Hoch, J. C.; Stern, A. S. *NMR Data Processing*; Wiley: New York, 1996.
(62) Jaravine, V.; Ibraghimov, I.; Orekhov, V. Y. *Nat. Methods* **2006**, *3*, 605−607.